SCIENCE CHINA
Earth Sciences

Uplift and exhumation in the Tianshan, western China: New insights from detrital zircon morphology and thermochronology

Jian CHANG[1,2,*], Yinglin ZHANG[1,2], Nansheng QIU[1,2,†] and Chenxing LI[1,2]

Citation: SCIENCE CHINA Earth Sciences **65**, 449 (2022); doi: 10.1007/s11430-021-9872-4

View online: https://engine.scichina.com/doi/10.1007/s11430-021-9872-4

View Table of Contents: https://engine.scichina.com/publisher/scp/journal/SCES/65/3

Published by the Science China Press

SCIENCE CHINA
Earth Sciences

•RESEARCH PAPER•

March 2022 Vol.65 No.3: 449–461
https://doi.org/10.1007/s11430-021-9872-4

Uplift and exhumation in the Tianshan, western China: New insights from detrital zircon morphology and thermochronology

Jian CHANG[1,2*], Yinglin ZHANG[1,2], Nansheng QIU[1,2†] & Chenxing LI[1,2]

[1] *State Key Laboratory of Petroleum Resources and Prospecting, China University of Petroleum, Beijing 102249, China;*
[2] *College of Geosciences, China University of Petroleum, Beijing 102249, China*

Received August 25, 2021; revised November 16, 2021; accepted November 23, 2021; published online January 4, 2022

Abstract The Tianshan in western China is rich in ore resources, but its tectonic uplift and exhumation history closely related to the resource exploration is still controversial. This study provides a new strategy to uncover the tectonic uplift processes in southern Tianshan by combining the morphological characteristics and thermochronological ages of detrital zircons in the Tarim Basin. The morphology of the Meso-Cenozoic detrital zircons in the Kuqa Foreland Basin, a secondary tectonic unit of the Tarim Basin, is dominated by three types of P, S, and G, and their average alkaline and temperature indexes are 668.0−677.2 and 347.6−413.5, respectively. Moreover, the U-Pb ages of these detrital zircons are primarily divided into two groups of 270−330 and 380−470 Ma. These features indicate that the Early Carboniferous-Early Permian and Middle Ordovician-Middle Devonian alkaline granites distributed in the South Tianshan and southern Central Tianshan were the main sources of the detrital zircons in the Kuqa Foreland Basin. The decomposition of the detrital zircon fission track ages further reveals that the provenances of the Kuqa Foreland Basin primarily consisted of the southern Central Tianshan, the eastern South Tianshan, and the central South Tianshan during Meso-Cenozoic. Among them, the eastern South Tianshan played a dominant role in the material supply. The synthesis of the decomposed zircon fission track (ZFT) ages and the lag-time evolution pattern indicated that the South Tianshan and the southern Central Tianshan mainly experienced five stages of tectonic uplifting that occurred in the Devonian, the Permian, the Middle Triassic-Middle Jurassic, the Cretaceous, and since the Miocene, respectively. They were related to the subduction of the South Tianshan Ocean northward to the bottom of the Central Tianshan, the compression and accretion after the closure of the South Tianshan Ocean, and a series of collisions between the Qiangtang-Lassa-India plates and the southern margin of the Eurasia plate in the Meso-Cenozoic, respectively. This study provides a new provenance analysis method, which was successfully applied in the Tianshan, and also develops a new way to study Central Asia's tectonic evolution.

Keywords Tianshan, Kuqa Foreland Basin, Provenance analysis, Zircon morphology, Thermochronology, Lag-time evolution

Citation: Chang J, Zhang Y, Qiu N, Li C. 2022. Uplift and exhumation in the Tianshan, western China: New insights from detrital zircon morphology and thermochronology. Science China Earth Sciences, 65(3): 449–461, https://doi.org/10.1007/s11430-021-9872-4

1. Introduction

The exhumation materials produced by orogenic belts can be rapidly transported to adjacent foreland basins for deposition by wind and river forces, so the uplift and exhumation processes of orogenic belts are interdependent with the subsidence of foreland basins. When the exhumed apatite and zircon minerals from orogenic belts transported to the sedimentary basins were buried very shallow with burial temperatures lower than their thermochronological closure temperatures, they will retain the thermal information of the provenances and can be effectively used to study the uplifting histories of the provenances (orogenic belts) and basin-mountain coupling relationship (Garver et al., 1999; Bernet and Garver, 2005; Carrapa, 2009; Qiu et al., 2012).

* Corresponding author (email: changjian@cup.edu.cn)
† Corresponding author (email: qiunsh@cup.edu.cn)

The decomposition analysis of the unreset low-temperature thermochronological ages for detrital minerals can initially identify their provenances (orogenic belts) and uplifting events, and the correlation among the decomposed low-temperature thermochronological peak ages, stratigraphic ages, and lag-time can be used to study the tectonic evolution stages and exhumation rates of the orogenic belts (Garver et al., 1999; Bernet and Garver, 2005; Carrapa, 2009). They have been successfully applied in the Alps, Tibet Plateau, and Taiwan Central Mountains (Garver et al., 1999; Bernet et al., 2001; Bernet and Garver, 2005; Carrapa, 2009; Carrapa et al., 2016; Malusà and Fitzgerald, 2020).

Similar to the Alps and the Tibet Plateau, the Tianshan in western China (especially the southern Tianshan) also experienced long-term uplifting and exhumation. The exhumation materials were then rapidly transported to the foreland basins in the southern margin of the Tianshan for deposition. Therefore, it is feasible to carry out the provenance analysis of Meso-Cenozoic detrital rocks from the Kuqa Foreland Basin (KFB) in the south margin of the Tianshan with a thermochronological method. Previous studies discussed the tectonic uplifting processes of the South Tianshan since the Cretaceous by apatite fission track and (U-Th)/He ages of bedrock samples in the Tianshan and the northern KFB, but the conclusions are still controversial (Yin et al., 1998; Huang et al., 2006; Wang et al., 2009; Chang et al., 2017, 2021). According to the analyses on detrital zircon U-Pb ages, heavy minerals, and whole-rock main elements, it has been confirmed that the South Tianshan was the primary provenance for the KFB during the Meso-Cenozoic (Li et al., 2004a; Li et al., 2006; Li and Peng, 2010; Liu et al., 2013), but other geological information contained in detrital sediments has not been extracted. Compared with the methods mentioned above, the unreset fission track ages of the Meso-Cenozoic detrital zircons in KFB can not only reveal the tectonic evolution history of the Tianshan before the Cretaceous but also provide new evidence for the tectonic uplift events since the Cretaceous, which would be significative to understand the relationship among structure, landform, denudation, and deposition in Tianshan. In this study, we first show that the southern Tianshan is the primary provenance of the KFB during the Meso-Cenozoic based on the morphological characteristics and U-Pb ages of the detrital zircons. Then the number, uplifting events, and exhumation rates of the provenances were studied with the decomposition and lag-time evolution pattern analysis on detrital zircon fission track (ZFT) ages. Finally, we synthetically discussed the provenance domains and the causes for the multiple uplifting events. This paper not only provides a new provenance analysis method and first uncovers the multiple cooling events that occurred in the South Tianshan after the closure of the South Tianshan Ocean, but also verifies the validity of the detrital thermochronology for provenance analysis in the Tianshan, and thus develops a new way to study Central Asia's tectonic evolution.

2. Geological setting and samples' information

The studied areas in this study include the southern Tianshan and the KFB in the northern Tarim Basin. As part of the Central Asian orogenic belt, the Tianshan is bounded by the Tarim Basin to the south and Junggar Basin to the north. The Tianshan is divided into the eastern and western Tianshan separated by the Urumqi-Korla line; the western Tianshan can be divided further into three domains (Figure 1a): the North, Central (including the Yili Block), and South Tianshan. The Central Tianshan belongs to a magmatic arc and consists of volcanic rocks and granites developed from Ordovician to Carboniferous (Gao et al., 2009). The South Tianshan in the south of the Central Tianshan began to develop along with the collision between the Central Tianshan island arc and Tarim Block during the Late Carboniferous-Early Permian (Xiao et al., 2004; Han et al., 2011; Ge et al., 2012). The Precambrian, lower and upper Paleozoic strata in the South Tianshan were characterized by epimetamorphic rock, marine volcanic-sedimentary formation, and alternative marine-continental volcanic-sedimentary formation, respectively (Chen et al., 1983).

The KFB in the northern Tarim Basin is bounded by the South Tianshan to the north and the Tabei Uplift (one secondary tectonic unit of the Tarim Basin) to the south. It is divided into five secondary structural units from north to south: the Northern Monocline Belt, the Kelasu-Yiqikelike Thrust Belt, the Baicheng Sag, the Yangxia Sag, and the Qiulitag Anticline Belt (Figure 1b). The KFB developed on the Paleozoic fold basement and experienced three evolutionary stages: Late Permian-Triassic foreland basin, Jurassic-Paleogene extensional depression basin, and Neogene-Quaternary rejuvenated foreland basin (He et al., 2004; He et al., 2009). The strata in the KFB can be divided into three sequences as the gypsum-salt rock in the Paleocene-Eocene Kumugeliemu group serves as a mark layer (Tang et al., 2004). The Triassic, Jurassic, and Lower Cretaceous strata below the mark layer mainly consist of continental conglomerate, sandstone, and mudstone; the lithology of the mark layer is characterized by gray-light gray salt rock, gypsum rock, limestone, marlstone, mudstone, sandstone, and sandy conglomerate; the strata above the mark layer consist of Oligocene-Quaternary red clastic rocks.

We collected six detrital rocks for this study from the Lower Jurassic, Lower Cretaceous, Paleocene, Oligocene, Miocene, and Quaternary strata in the outcrop of the Yaha Section in the eastern KFB. The location and geological information of these samples are shown in Figure 1c and Table 1, respectively. The zircon minerals from these sam-

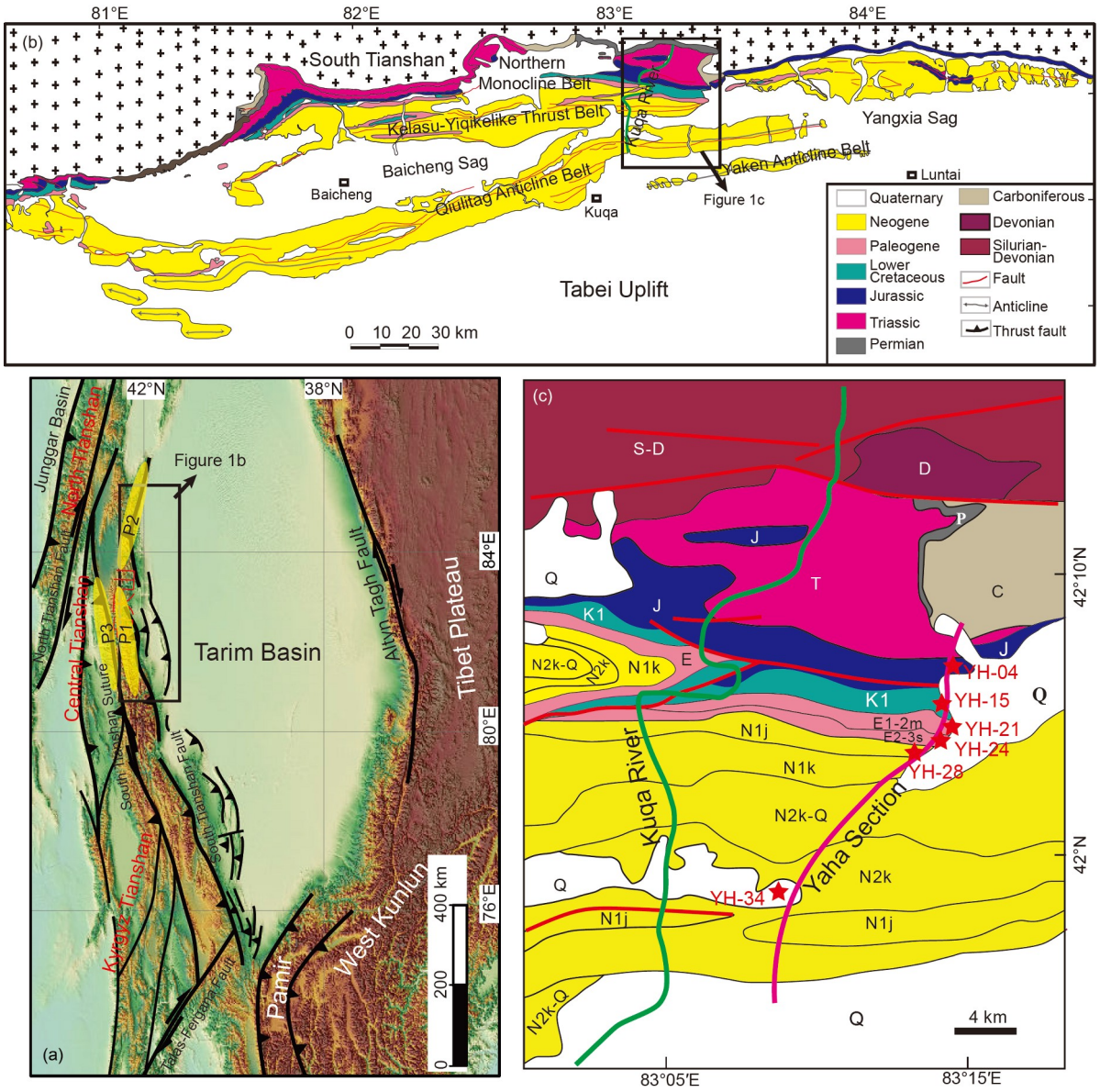

Figure 1 (a) Geomorphologic map of Central Asia with some primary faults. Yellow areas represent the three provenances identified in this study; (b) geological map of the KFB showing five secondary structural units; (c) geological map of the Yaha Section in the eastern KFB showing the samples' locations (red stars).

ples by heavy mineral separation technology were used to measure the morphology, U-Pb ages, and fission track ages. The experiment methods and measured results of the zircon U-Pb and fission track dating were shown in the Appendix (https://link.springer.com).

3. Meso-Cenozoic provenance analysis in the KFB

The Meso-Cenozoic detrital zircon fission track ages and their lag-time evolution pattern in the KFB could be used to study the tectonic uplifting history of the southern Tianshan if these detrital zircons in the KFB were confirmed to come from the Tianshan. As mentioned above, previous studies have concluded that the South Tianshan became the essential provenance of the KFB since the Mesozoic by analyzing the sandstone skeleton grains, heavy minerals, and whole-rock major elements (Li et al., 2004a, 2006; Li and Peng, 2010). This study did detailed work on the detrital zircon morphological characteristics and U-Pb ages of the Meso- Cenozoic samples in the Yaha Section to further clarify the provenances of the eastern KFB.

3.1 Morphological characteristics of the detrital zircons

Due to the variation of their host magma's chemical com-

Table 1 Basic information of the samples from the Yaha Section in the eastern KFB and the detrital zircons' morphology and fission track data

Sample No.	Stratigraphic age (Ma)	Formation	Lithology	Altitude (m)	Coordinate	$I.\overline{A}$ [a)]	$I.\overline{T}$ [b)]	N [c)]	Single-grain ZFT age (Ma)	ZFT central age (Ma)	$P(\chi^2)$ [d)]	P1	P2	P3
YH-04	190±5	Lower Jurassic	Fine sandstone	2066	42°7′43.3″N; 83°24′49.5″E	668.0	391.6	88	185–549	295.5±7.7	0	225.0±7.5 (29.0%)	293.4±8.8 (44.0%)	399.5±10.1 (27.0%)
YH-15	120±5	Lower Cretaceous	Siltstone	1852	42°5′1.6″N; 83°23′15.3″E	668.0	371.1	82	110–484	266.8±9.5	0	177.5±3.8 (28.5%)	274.5±9.8 (35.9%)	362.2±11.9 (35.6%)
YH-21	55±5	Paleocene	Fine sandstone	1810	42°4′18.2″N; 83°23′58.4″E	668.8	409.5	81	103–568	236.9±10.1	0	130.3±4.9 (19.4%)	232.6±5.0 (51.2%)	365.0±9.8 (29.4%)
YH-24	30±3	Oligocene	Pebbly sandstone	1782	42°4′6.7″N; 83°23′50.3″E	671.6	413.5	132	105–466	276.5±8.7	0	120.4±4.3 (5.2%)	207.9±2.4 (40.8%)	373.1±3.2 (54.0%)
YH-28	18±3	Miocene	Fine sandstone	1690	42°3′0.6″N; 83°21′15.7″E	675.1	347.6	119	60–452	189.7±7.0	0	98.1±2.9 (16.2%)	175.6±2.6 (49.7%)	283.2±4.4 (34.1%)
YH-34	1.5±0.3	Quaternary	Conglomerate	1503	41°59′34.0″N; 83°19′0.7″E	677.2	381.2	29	60–331	137.2±13.0	0	73.2±3.2 (21.3%)	116.5±3.4 (47.6%)	267.9±7.6 (31.1%)

a) Average alkaline index; b) average temperature index; c) zircon grain number; d) chi-square probability.

position, temperature, and aluminum-alkali index, zircon crystals can form different morphology during crystallization. In addition, because zircon grains have strong resistance to weathering and metamorphism, they are usually preserved in good original morphology after weathering, transportation, and deposition. According to the combination relationship of different cylindrical and conical surfaces of zircon crystals and their development degree, Pupin (1980) divided zircon morphology into 16 primary types and 64 subtypes and designed a zircon morphology distribution diagram (Figure 2). The *X*-axis represents alkaline index (*I.A*), and the *Y*-axis represents temperature index (*I.T*). These two indexes range from 100 to 800 and are divided further into eight equal parts. The temperature index increases from top to bottom, while the alkaline index increases from left to right. In this study, we analyzed more than 1200 zircon grains' morphology of six samples from the Yaha Section and then plotted the statistical frequency into the zircon morphology distribution diagrams (Figure 3), showing that the zircon morphology is dominated by three types of P (P1 or P2), S and G. Meanwhile, the average alkaline index ($I.\overline{A}$) and temperature index ($I.\overline{T}$) of each sample were calculated by formulas (1) and (2) proposed by Pupin (1980) (Table 1).

$$I.\overline{A} = \sum_{I.A=100}^{800} I.A \times n_{I.A}, \quad (1)$$

$$I.\overline{T} = \sum_{I.T=100}^{800} I.T \times n_{I.T}, \quad (2)$$

where *I.A* is the alkaline index for a certain zircon morphology, $n_{I.A}$ is the statistical frequency of a certain zircon morphology corresponding to the alkaline index, *I.T* is the temperature index for a certain zircon morphology, and $n_{I.T}$ is the statistical frequency of a certain zircon morphology corresponding to the temperature index.

The $I.\overline{A}$ and $I.\overline{T}$ values of the Meso-Cenozoic samples from the Yaha Section in the KFB range from 668.0 to 677.2 and from 347.6 to 413.5, respectively. When the average alkaline and temperature indexes of each sample were plotted into the parent rock type chart (Figure 3g), these detrital zircons were mainly derived from alkaline granites. This is consistent with the exposure of alkaline granites in the Kuerchu and Boziguoer areas of the South Tianshan, Central Tianshan, and Yili area (Liu et al., 2014; Qin, 2017; Han and Zhao, 2018; Huang et al., 2020). Therefore, the Tianshan was the main provenance of the Yaha Section during the Meso-Cenozoic.

3.2 Detrital zircon U-Pb ages

The detrital zircon U-Pb ages of samples YH-04, YH-15, YH-21, YH-24, and YH-28 were obtained for identifying the provenances of the Meso-Cenozoic sediments from the Yaha Section in the eastern KFB. For the Lower Jurassic sample YH-04, the U-Pb ages of 111 zircon grains range from 301 to 2454 Ma (Figure 4a), and 83% of the zircon grains are further classified as a group with U-Pb ages of 380–470 Ma (peak age of 418.6 Ma). For the Lower Cretaceous sample YH-15, except for one zircon U-Pb age of 1954±75 Ma, the U-Pb ages of the other 43 zircons range from 242 to 500 Ma and can be further divided into three groups of 242–250 Ma (18%, peak age of 247.5 Ma), 271–308 Ma (23%, peak age of 280.5 Ma) and 381–500 Ma (55%, peak age of 443.3 Ma) (Figure 4b). For Paleocene sample YH-21, the U-Pb ages of 112 zircon grains range from 202 to 2770 Ma (Figure 4c), and the two largest groups are 270–325 Ma (17%, peak age of 300 Ma) and 400–470 Ma (38%, peak age of 424.5 Ma). For Oligocene sample YH-24, except for four zircon ages of >500 Ma, the U-Pb ages of the residual 108 zircon grains range from 263 to 461 Ma (Figure 4d) and are divided into two groups of 281–308 Ma (29%, peak age of 299.2 Ma) and 409–461 Ma (66%, peak age of 424.6 Ma). For Miocene sample YH-28, the U-Pb ages of 164 zircon grains range from 238 to 2514

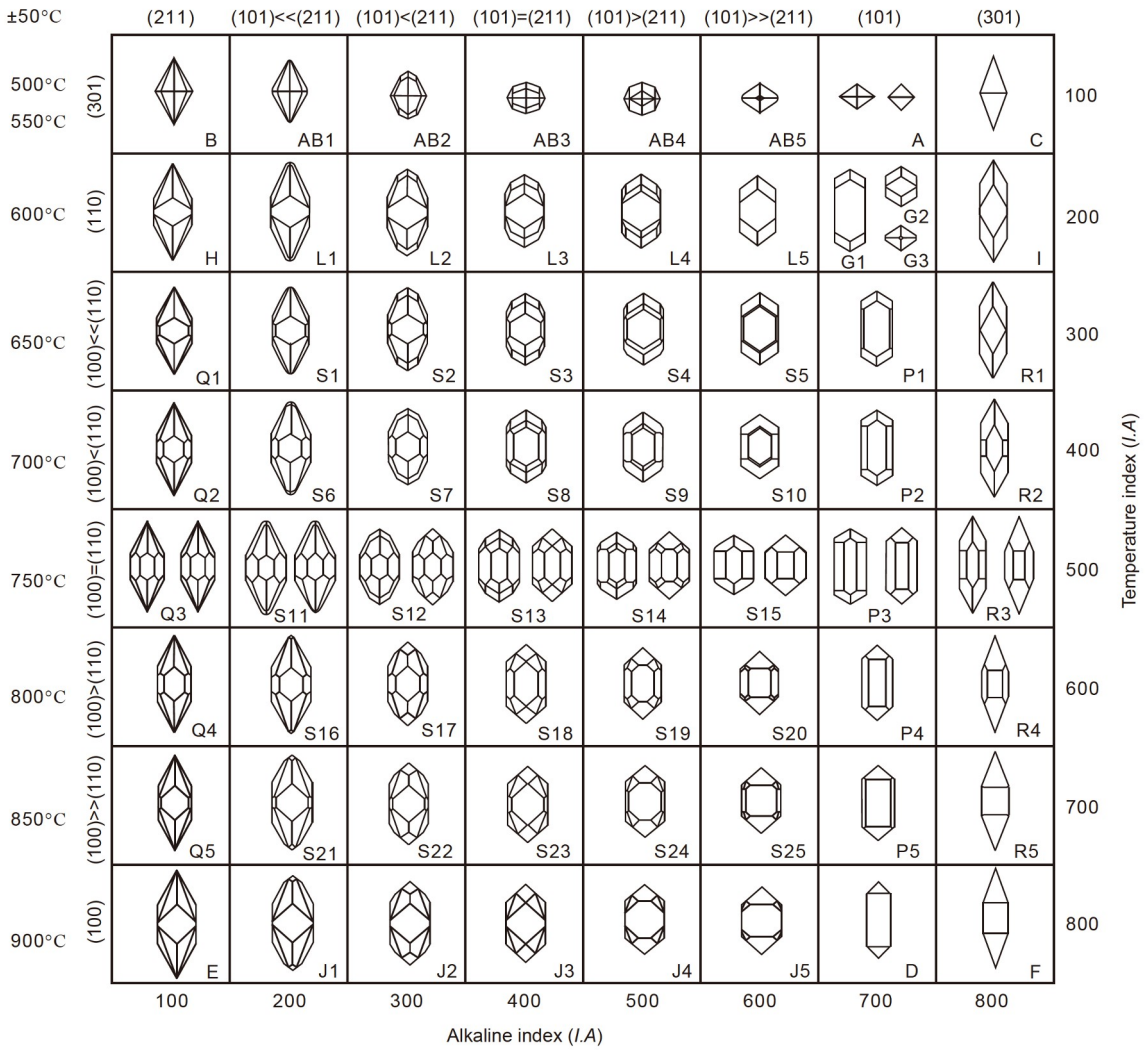

Figure 2 Distribution diagram of the zircon morphology (Pupin, 1980).

Ma (Figure 4e), and the two largest groups are 270–336 Ma (13%, peak age of 300.3 Ma) and 400–447 Ma (46%, peak age of 426.4 Ma).

According to previous studies on zircon U-Pb ages of the bedrock in the Tianshan and surrounding mountains, we concluded that the detrital zircons with the U-Pb ages of 202−250 Ma in the Yaha Section were probably derived from the West Kunlun Mountain, Kuruktag Mountain or Beishan Mountain, which are far from the KFB (Liu et al., 2013; Han and Zhao, 2018); The detrital zircons with the U-Pb ages of 270−330 Ma came from granites in the south Tianshan and the southern Central Tianshan, which developed with the collision between the Central Tianshan and Tarim blocks during Early Carboniferous-Early Permian (Liu et al., 2013; Qin, 2017; Han and Zhao, 2018); The detrital zircons with the U-Pb ages of 380−470 Ma were probably supplied by the granites in the southern Central Tianshan and northern South Tianshan, which were related to the tectonic accretion between the Central Tianshan and South Tianshan Ocean inducing magmatic activities during Middle Ordovician-Middle Devonian (Wang et al., 2011; Han et al., 2011; Qin, 2017). The detrital zircons with the U-Pb ages >500 Ma were derived from the cyclic sediments of the ancient basements in the Tianshan and the northern margin of the Tarim Basin, which were too few to be further discussed in this study. The detrital zircon U-Pb ages of all the samples were dominantly divided into two groups of 270–330 Ma with a peak age of 300 and 380–470 Ma with a peak age of 424.5 Ma (Figure 4f), indicating that the South Tianshan and southern Central Tianshan are the most important provenances for the KFB during Meso-Cenozoic. The Lower Jurassic strata in the Yaha Section are short of zircon U-Pb ages of 270–330 Ma, similar to the Kuqa River Section in the middle of the KFB (Li and Peng, 2010). The Early Carboniferous-Early Permian magmatic rocks in the South Tianshan and surrounding areas might not be exposed during the Early Jurassic. Therefore, they could not provide the detrital materials for the KFB.

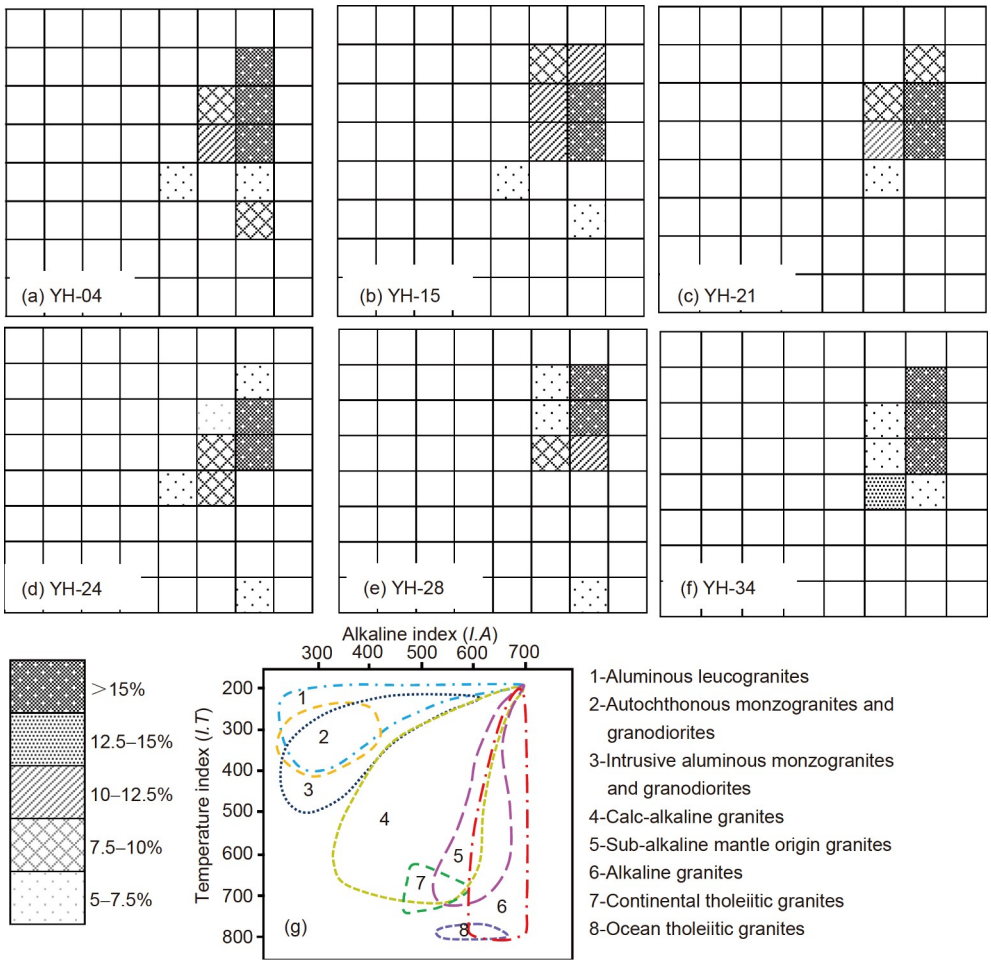

Figure 3 (a)–(f) Statistics diagrams of detrital zircons' morphology of the Meso-Cenozoic samples from the Yaha Section in the KFB; (g) parent rock identification chart with the samples' points (red circles).

4. Analysis on the zircon fission track ages

The central ZFT ages of the six samples in this study range from 137.2 to 295.5 Ma (Table 1) and are older than the corresponding stratigraphic ages. Their $P(\chi^2)$ values were all equal to 0. These features indicate that the Meso-Cenozoic sediments in the Yaha Section did not experience high temperatures after their deposition. Their ZFT ages have been unreset and still record the thermal information of the provenances (southern Central Tianshan and South Tianshan). The samples' single-grain ZFT ages exhibit a nonlinear negative correlation with uranium contents (Figure 5a), indicating that the radiation damage probably affects the ZFT ages' dispersion. The youngest single-grain ZFT ages for each sample gradually increased from the Early Jurassic to the Quaternity (Figure 5b), implying that the provenances experienced continuous exhumation since the Early Jurassic, which caused the thermochronological ages of the bedrock in the origins to become younger gradually. The central ZFT ages of the unreset samples have no geological significance. Some studies proposed the decomposition method to analyze the single-grain ZFT ages of the diverse sources for extracting thermal information (Galbraith and Green, 1990; Brandon et al., 1998; Brandon, 2002; Vermeesch, 2018). The decomposition method can effectively identify the provenance number of the detrital ZFT ages and reveal the uplifting events experienced by each provenance. In this study, the Binomial "peaking-fitting" method proposed by Galbraith and Green (1990) was used to decompose the single-grain ZFT ages of each sample. It is found that only when each sample was subdivided into three groups, the test parameters, including χ^2 statistics and P(F), could achieve the best results (Brandon, 2002). Therefore, the single-grain ZFT ages of each sample were subdivided into three groups of P1, P2, and P3 from young to old (Table 1), indicating three provenances (corresponding to I, II, and III) in the Yaha Section since the Jurassic. The peak ZFT ages of the three groups for all the samples gradually become smaller as the stratigraphic ages get younger, implying that the uplifting and exhumation processes of these three provenances were progressive. The further statistical analysis on the decomposed peak ZFT ages revealed that the Tianshan experienced

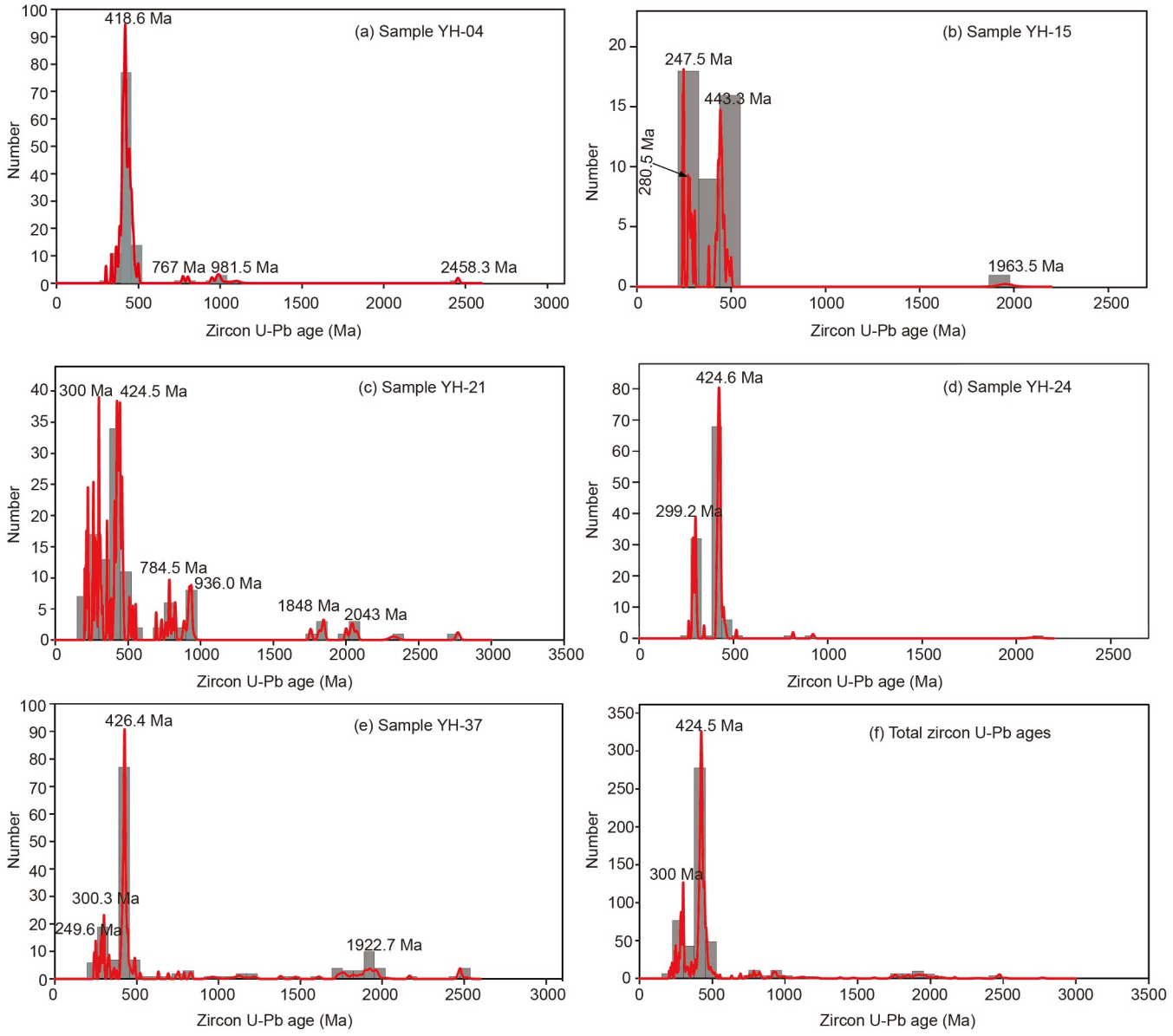

Figure 4 Histograms of the Meso-Cenozoic detrital zircons from the Yaha Section in the KFB.

four cooling events from Devonian to Cretaceous, which occurred in 399.5−362.2, 293.4−267.9, 232.6−175.6, and 130.3−73.2 Ma, respectively. The lag-time evolution pattern of the ZFT ages will be established in the next section to reveal Tianshan's tectonic uplifting since the Cenozoic.

5. Lag-time evolution pattern of ZFT ages

When zircon crystals did not experience partial or complete annealing after deposition in sedimentary basins, the value of the measured ZFT age minus the corresponding stratigraphic age is defined as a lag-time (Garver et al., 1999). In this study, the lag-time evolution pattern between the recomposed ZFT ages and corresponding stratigraphic ages for the samples in the Yaha Section was established in Figure 6. There are three fundamental trends between the thermochronological ages line and lag-time contours (Figure 7a). The first trend is that the thermochronological age line is more inclined than the lag-time contour, indicating an accelerated exhumation and orogenic stage in the provenance (Constructive). The second trend is that the thermochronological age line is parallel to the lag-time contour, indicating a constant exhumation stage in the provenance (Steady-state). The third trend is that the thermochronological age line is less inclined than the lag-time contour, which means slowing exhumation rates in the provenance (Decaying). As shown in Figure 6, the variation trend of the ZFT peak ages in group P1 suggests that the provenance I experienced a slowly decaying stage from the

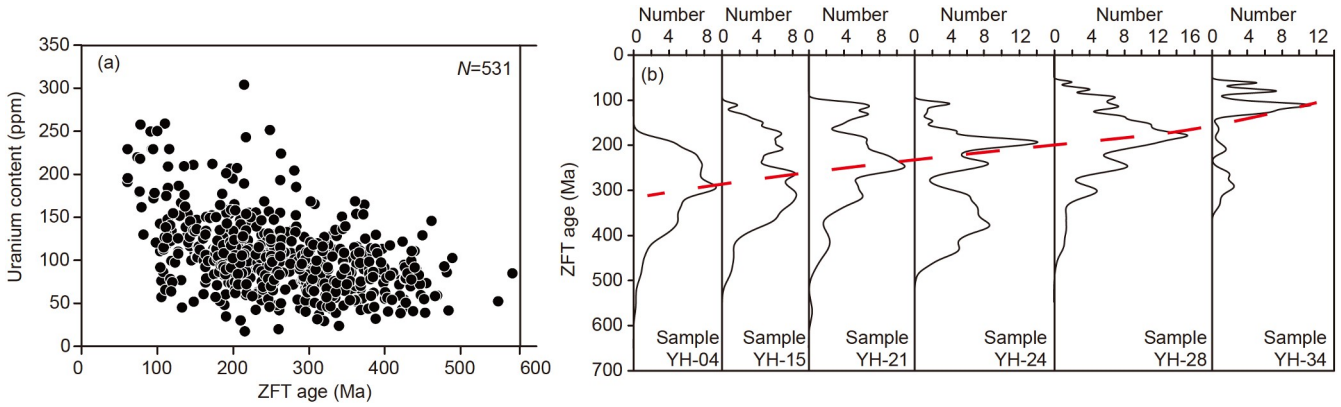

Figure 5 (a) Correlation of the single-grain ZFT ages of the Meso-Cenozoic samples in the Yaha Section with the uranium content; (b) probability distribution of each sample's single-grain ZFT ages.

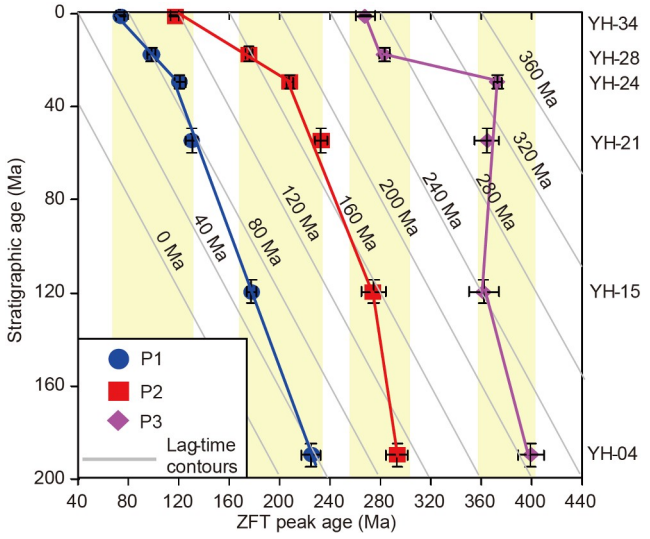

Figure 6 Correlation of the ZFT peak ages and corresponding stratigraphic ages of the samples from the Yaha Section in the KFB and their lag-time evolution pattern. The yellow zones represent the time span of four uplifting events.

Early Jurassic to the Oligocene and a rapid uplifting phase since the Oligocene. The variation trend of the ZFT peak ages in group P2 suggests the provenance II experienced a slowly decaying stage from the Early Jurassic to the Early Cretaceous, a steady-state stage (Early Cretaceous to Oligocene), and a rapid uplifting stage since the Oligocene. The variation trend of the ZFT peak ages in group P3 suggests that the provenance III experienced a decaying stage from the Early Jurassic to the Oligocene, a rapid uplifting and orogeny stage from the Oligocene to the Miocene, and a steady-state stage since the Miocene. Its early decaying stage can be further divided into a slowly decaying stage from the Early Jurassic to the Early Cretaceous and a rapid decaying stage from the Early Cretaceous to the Oligocene. The three provenances of the Yaha Section experienced differential tectonic evolution processes since the Early Jurassic. Nonetheless, they are generally characterized by the decaying and steady-state stage during the Early Jurassic-Oligocene and the constructive and steady-state stage since the Oligocene.

The lag-time can be used to calculate the exhumation rate of the provenance (Brandon et al., 1998; Garver et al., 1999; Bernet and Garver, 2005). According to the natural radiation damage model proposed by Brandon et al. (1998), the transformation of the lag-time to an exhumation rate was calculated by the Age2EDOT program and plotted in Figure 7b, indicating the negative correlation between the lag time and exhumation rate. As the lag-time increases, the exhumation rate will decrease. For group P1 (Provenance I), the exhumation rate decreased from 250 m Ma^{-1} during the Early Jurassic to 90 m Ma^{-1} during the Oligocene and then increased to 110 m Ma^{-1} during the Quaternary. For group P2 (provenance II), the exhumation rate decreased from 80 m Ma^{-1} during the Early Jurassic to 55 m Ma^{-1} during the Early Cretaceous and further to 50 m Ma^{-1} during the Oligocene, then increased to 70 m Ma^{-1} during the Quaternary. For group P3 (provenance III), the exhumation rate decreased from 38 m Ma^{-1} during the Early Jurassic to 33 m Ma^{-1} during the Early Cretaceous and further to 22 m Ma^{-1} during the Oligocene, then increased rapidly to 30 m Ma^{-1} in the Miocene. Since the Miocene, the exhumation rate in provenance III remained constant.

6. Discussion

6.1 The provenance identification

As mentioned above, the decomposed ZFT peak ages of groups P1, P2, and P3 revealed that Yaha Section in the eastern KFB received sediments from provenances I, II, and III during Meso-Cenozoic. For group P3, the four ZFT peak ages of 399–365 Ma indicate that provenance III experienced a rapidly cooling event during the Devonian. Previous studies considered that the South Tianshan began to form during Late Carboniferous-Early Permian (Xiao et al., 2004; Han et al., 2011; Ge et al., 2012), so it did not experience the Devonian cooling event. We concluded that these zircon grains

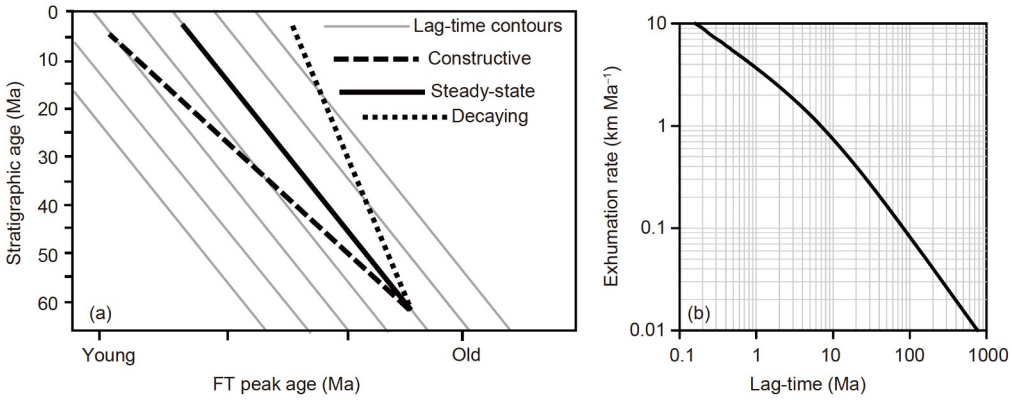

Figure 7 (a) Lag-time evolution pattern of the fission track ages (Bernet et al., 2001); (b) relationship of lag-time and exhumation rate (for the geothermal gradient of 25 °C km^{-1}).

in group P3 came from the southern Central Tianshan (Figure 8; Li and Peng, 2010). As a collision suture belt, the southern Central Tianshan is dominated by high-pressure metamorphic rocks with sporadic Silurian-Early Devonian granites (Zhu, 2007). The zircon grains of groups P1 and P2 probably came from the South Tianshan next to the KFB. Some studies indicated that the low-temperature thermochronological ages generally become older from the central South Tianshan to the eastern South Tianshan (Dumitru et al., 2001; Chang et al., 2021). One paleo-planation surface also developed in the eastern South Tianshan (Morin et al., 2019). These features indicate that the uplifting and exhumation rate in the eastern South Tianshan should be relatively smaller than that in the central South Tianshan. In addition, the most significant proportion of the single-grain ZFT ages for each sample belonged to group P2, which probably resulted from the convenience of the proximal supply. We finally concluded that the zircon grains in group P1 come from the central South Tianshan. In contrast, the eastern South Tianshan provided the zircon grains in group P2 with older ZFT peak ages (Figure 8). The central South Tianshan is characterized by clastic rocks and carbonate rocks developed during the Late Ordovician and Silurian with a few Early Carboniferous-Early Permian and Middle Ordovician-Middle Devonian magmatic rocks, while the eastern South Tianshan is dominated by upper Silurian-Carboniferous terrigenous clastic rocks and Paleozoic igneous rocks (Zhu, 2007). There are two functions to be responsible for the differential uplifting rates between the central and eastern South Tianshan since the Cenozoic: (1) the differential shortening rates between the central and eastern South Tianshan with the distant effect of the collision between the India Plate and the southern margin of the Eurasia Plate (Wang et al., 2001); (2) the upwelling of the hot asthenospheric mantle under the central South Tianshan (Lei and Zhao, 2007; Chang et al., 2021), which resulted in more rapidly uplifting in the central South Tianshan. The heavy mineral assemblages including zircon, rutile, and tourmaline developed in the Middle-Lower Jurassic strata of the KFB indicated that the Tianshan experienced weak tectonic activity and the South Tianshan is characterized by a low terrain during the Early-Middle Jurassic (Li et al., 2004b). The exhumation materials from the southern Central Tianshan were transported to the KFB by wind force, which was confirmed by the high content of Al_2O_3 in the Middle-Lower Jurassic strata (Li et al., 2005). Since the Late Jurassic, the differential uplifting between the Tianshan and the Tarim Basin allowed the development of intermountain river channels (Li et al., 2005), so the sediments in the KFB were transported from the Central Tianshan and South Tianshan by the rivers since the Late Jurassic.

6.2 Differential uplifting processes in the southern Tianshan

This study reveals the multiple tectonic uplifting events that occurred in the southern Tianshan since the Devonian by combining the decomposed ZFT ages and lag-time evolution pattern. The decomposed ZFT ages from the Yaha Section in the eastern KFB recorded the earliest Devonian cooling events (399–365 Ma) occurred in the southern Central Tianshan, which was earlier than that recorded by the muscovite $^{40}Ar/^{39}Ar$ plateau age of 359–356 Ma from the Heiyingshan Section in the South Tianshan (Wang et al., 2011). In addition, Glorie et al. (2010) considered that the Kyrgyz Tianshan experienced slowly cooling during the Late Devonian based on K-feldspar $^{40}Ar/^{39}Ar$ plateau ages. During the Devonian, the South Tianshan Ocean plate subducted northward below the Central Tianshan block, which not only induced upwelling of the asthenospheric mantle in the Central Tianshan through the slab rollback and formed massive magmatic rocks (Wang et al., 2020), but also caused the uplifting and exhumation in the shallow of the southern Central Tianshan (Tan et al., 2019; Huang et al., 2020), which were probably recorded by the zircon crystals of the deep strata in the southern Central Tianshan. During the Early Jurassic, these zircon minerals

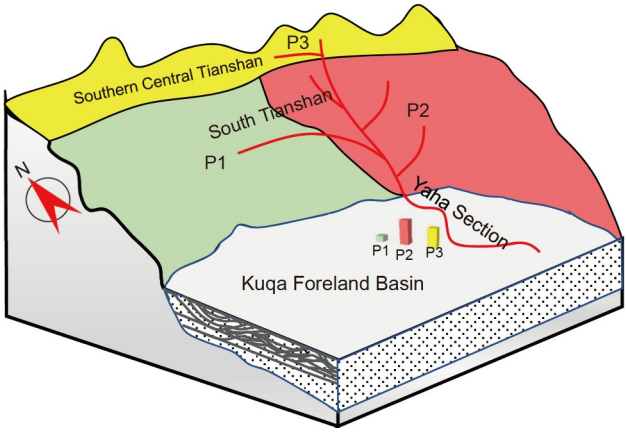

Figure 8 Schematic illustration of the Meso-Cenozoic provenances in the eastern KFB.

from the deep strata in the southern Central Tianshan were denuded and transported to the Yaha Section.

The Permian cooling event (293.4–267.9 Ma) revealed by the ZFT ages of groups P2 and P3 was also reported by analyzing $^{40}Ar/^{39}Ar$, zircon (U-Th)/He, and titanite fission track ages of bedrocks in the South Tianshan and Central Tianshan (Carroll et al., 1995; Dumitru et al., 2001; de Jong et al., 2009; Jolivet et al., 2010; Yin et al., 2018), which was related to the compression and accretion after the collision between the Central Tianshan and Tarim blocks. This cooling event not only resulted in the formation of massive mylonite along the South Tianshan suture belt with the effect of the dextral strike-slip faults but also generated a regional unconformity between Permian and its underlying strata in Central Asia (Carroll et al., 1995). Noted that some single-grain ZFT ages in groups P1, P2, and P3, which also recorded the Devonian and Permian cooling events, would be caused by the magmatic activity at that time. Due to the differential closure temperatures, these ZFT ages should be slightly different from the zircon U-Pb ages. This question should be further studied in the future.

The Middle Triassic- Middle Jurassic rapid uplifting event (232.6–175.6 Ma) in the South Tianshan revealed by groups P1 and P2 showed a corresponding relation with the rapid subsidence in the northern margin of the KFB, reflecting an excellent source-sink system (Li and Peng, 2010; Chang et al., 2017; Morin et al., 2018). Except for the South Tianshan, the low-temperature thermochronological data in the Central Tianshan, Kyrgyz Tianshan, Kunlun Mountain, Tibet Plateau, and Kalpin fold-and-thrust belt in the northern margin of the Tarim Basin also recorded this cooling event (Glorie et al., 2010; Cao et al., 2015; Jolivet, 2015), which probably resulted from the collision between the Qiangtang terrane and the southern margin of the Eurasia plate during the Late Triassic-Early Jurassic. This collision event reactivated the inherited Paleozoic structures in Tianshan, Tarim Basin, and Junggar Basin (Jolivet et al., 2010). It also led to the development of the foreland basins in the southwest Tarim Basin (Chang et al., 2019). During the same period, the Kalpin and Bachu areas in the Tarim Basin became the frontal uplifted areas of the foreland basins and underwent significant exhumation (Chang et al., 2019). Noted that the collision effect gradually weakened since the Early Jurassic, the South Tianshan was in the decaying stage with the decreased exhumation rates as revealed by the lag-time evolution pattern of the ZFT ages. Morin et al. (2018) suggested that the South Tianshan was denuded to become paleo-plain relief during the Early-Middle Jurassic.

The detrital ZFT ages in the KFB recorded the Cretaceous cooling event (130.3–73.2 Ma) occurred in the South Tianshan, which was also revealed by different kinds of thermochronological data in the Central Tianshan, Kyrgyz Tianshan, Kunlun Mountain, northern margin of the Tarim Basin, and the western margin of the Junggar Basin (Dumitru et al., 2001; Glorie et al., 2010; Jolivet et al., 2010; Glorie and De Grave, 2016; Yin et al., 2018). This cooling event was related to the collision between the Lhasa terrane and the southern margin of the Eurasia plate (Dumitru et al., 2001; Jolivet et al., 2010). According to the thermal modeling and geological information, Morin et al. (2019) and Jolivet (2015) considered that most of Central Asia developed a paleo-planation surface and experienced slow uplifting and exhumation during the Late Jurassic-Early Cenozoic. At that time, the eastern South Tianshan developed to a paleo-planation surface as revealed by the ZFT ages with slowly cooling, which is the same as that shown by the lag-time evolution. The central South Tianshan was a structural reactivation region or influenced by the regional strike-slip faults (Jolivet et al., 2010; De Grave et al., 2013). Therefore, the central South Tianshan experienced more rapidly uplifting during the Cretaceous.

The rapid cooling event since the Oligocene (or the Miocene) revealed by the lag-time evolution pattern was also recorded by the sedimentary facies transition, paleomagnetic data, and thermochronological data of many orogenic belts and their piedmont fold-and-thrust belts in Central Asia (Yin et al., 1998; Dumitru et al., 2001; Huang et al., 2006; Jolivet et al., 2010; Macaulay et al., 2014; Chang et al., 2017, 2019). It was caused by the distant effect of the collision between the India plate and the southern margin of the Eurasia plate (Yin et al., 1998; Dumitru et al., 2001). During the late Cenozoic, the South Tianshan not only experienced rapidly uplifting with the exhumation rates of 90–110 m Ma^{-1} but also began subducting southward under the influence of tectonic compression and finally resulted in the development of the Kashi, Kalpin, and Kuqa fold-and-thrust belts in the northern margin of the Tarim Basin (Dumitru et al., 2001; Chang et al., 2019). Some studies suggested that the exhumation rates of the South Tianshan since the Miocene were 130–200 m Ma^{-1} based on apatite fission track analy-

sis, which is slightly larger than this study. Previous studies considered that the shortening deformation in the northern margin of the Tarim Basin initiated at 20–25 Ma (Yin et al., 1998; Dumitru et al., 2001; Chang et al., 2017), which is slightly later than the rapid uplifting time of the South Tianshan gotten from this study. It is implied that the vertical deformation in the South Tianshan is ahead of lateral deformation. The paleomagnetic data of the Miocene samples in the Yaha Section revealed that the South Tianshan experienced two rapid uplifting events of 17–16 and 11 Ma (Huang et al., 2006; Charreau et al., 2006), which were not revealed by the lag-time evolution pattern of the ZFT ages. It is probably because the limited samples were unable to precisely constrain the tectonic deformation process in the South Tianshan since the Miocene.

6.3 Limitations of the detrital thermochronological lag-time evolution pattern

The accuracy of the lag-time evolution pattern is affected by the low-temperature thermochronological ages and the stratigraphic ages of the samples. Moreover, the accuracy of the ZFT ages mainly depends on the experiment testers and the estimated grain amounts. Therefore, the testers should be careful for running the experiments and counting zircon grains as many as possible to obtain more accurately recomposed ZFT ages. The stratigraphic ages of the samples can affect the slope of the ZFT ages variation trend. Due to the lack of paleomagnetic constraints on the stratigraphic ages in the Yaha Section, we gave an error of 5–10% for the stratigraphic age of each sample, which would improve the analytical reliability. Carrapa (2009) clarified the correlation between the thermochronological lag-time evolution pattern and the orogenic wedge thrusting style, which was opposed by Bernet (2010). Bernet (2010) considered that the different thermochronometers manifest different sensitivities for the tectonic evolution of the upper crust and, therefore should provide different responses for the variation of exhumation rate. In addition, fission track samples from bedrocks in orogenic belts always experience the evolutionary process of no annealing, partial annealing, or full annealing along with the exhumation. If these samples were transported and deposited in the sedimentary basins, their fission track ages did not experience annealing after deposition. The evolution of fission track ages in the sedimentary basins should mirror the evolution pattern in the orogenic belts. This evolution pattern probably affects the lag-time evolution pattern and should be further studied in the future.

7. Conclusions

The southern Tianshan's tectonic uplifting and exhumation histories are innovatively studied based on the morphological characteristics and thermochronological ages of the Meso-Cenozoic detrital zircons in the KFB. The morphology of the detrital zircons is dominated by three types of P (P1 or P2), S, and G, and their corresponding average alkaline and temperature indexes are of 668.0−677.2 and 347.6−413.5, respectively. The detrital zircon U-Pb ages primarily cluster at 270−330 and 380−470 Ma. These features indicate that the Meso-Cenozoic detrital zircons in the KFB came from alkaline granites in the South Tianshan and southern Central Tianshan, which formed in the Early Carboniferous-Early Permian and Middle Ordovician-Middle Devonian. Furthermore, we identified three provenances: the southern Central Tianshan, eastern South Tianshan, and central South Tianshan, which experienced four uplifting and exhumation events in 399.5−362.2, 293.4−267.9, 232.6−175.6, and 130.3−73.2 Ma, respectively. These uplifting events were related to the northward subduction of the South Tianshan Ocean during the Devonian, collision, and compression after the closure of the South Tianshan Ocean during the Early Permian, and the collisions between the Qiangtang-Lassa plates and the southern margin of the Eurasia plate in the Mesozoic. During the Jurassic-Oligocene and the Miocene, the South Tianshan and southern Central Tianshan were in decaying and rapid uplifting orogenic stages (caused by the distant collision between India and Eurasia plates), respectively. Since the Early Jurassic, the central South Tianshan showed the maximum exhumation rates with 90–250 m km^{-1}.

Acknowledgements *We are grateful to the scientific editor Prof. Yuanbao WU and two anonymous reviewers for their constructive reviews of the initial manuscript. This work was supported by the National Natural Science Foundation of China (Grant Nos. 41972125 & U19B6003-02-03).*

References

Bernet M, Garver J I. 2005. Fission-track analysis of detrital zircon. Rev Mineral Geochem, 58: 205–237
Bernet M, Zattin M, Garver J I, Brandon M T, Vance J A. 2001. Steady-state exhumation of the European Alps. Geology, 29: 35–38
Bernet M. 2010. Tracing exhumation and orogenic wedge dynamics in the European Alps with detrital thermochronology: COMMENT. Geology, 38: e226
Brandon M T, Roden-Tice M K, Garver J I. 1998. Late Cenozoic exhumation of the Cascadia accretionary wedge in the Olympic Mountains, northwest Washington State. Geol Soc Am Bull, 110: 985–1009
Brandon M T. 2002. Decomposition of mixed grain age distributions using Binomfit. On Track, 24: 13–18
Cao K, Wang G C, Bernet M, van der Beek P, Zhang K X. 2015. Exhumation history of the West Kunlun Mountains, northwestern Tibet: Evidence for a long-lived, rejuvenated orogen. Earth Planet Sci Lett, 432: 391–403
Carrapa B, Di Giulio A, Mancin N, Stockli D, Fantoni R, Hughes A, Gupta S. 2016. Tectonic significance of Cenozoic exhumation and foreland basin evolution in the Western Alps. Tectonics, 35: 1892–1912
Carrapa B. 2009. Tracing exhumation and orogenic wedge dynamics in the European Alps with detrital thermochronology. Geology, 37: 1127–1130
Carroll A R, Graham S A, Hendrix M S, Ying D, Zhou D. 1995. Late

Paleozoic tectonic amalgamation of northwestern China: Sedimentary record of the northern Tarim, Northwestern Turpan, and southern Junggar Basins. Geol Soc Am Bull, 107: 571–594
Chang J, Glorie S, Qiu N, Min K, Xiao Y, Xu W. 2021. Late Miocene (10.0–6.0 Ma) rapid exhumation of the Chinese South Tianshan: Implications for the timing of aridification in the Tarim Basin. Geophys Res Lett, 48: e90623
Chang J, Li D, Min K, Qiu N, Xiao Y, Wu H, Liu N. 2019. Cenozoic deformation of the Kalpin fold-and-thrust belt, southern Chinese Tian Shan: New insights from low-T thermochronology and sandbox modeling. Tectonophysics, 766: 416–432
Chang J, Tian Y T, Qiu N S. 2017. Mid-Late Miocene deformation of the northern Kuqa fold-and-thrust belt (southern Chinese Tian Shan): An apatite (U-Th-Sm)/He study. Tectonophysics, 694: 101–113
Charreau J, Gilder S, Chen Y, Dominguez S, Avouac J P, Sen S, Jolivet M, Li Y, Wang W. 2006. Magnetostratigraphy of the Yaha section, Tarim Basin (China): 11 Ma acceleration in erosion and uplift of the Tian Shan mountains. Geology, 34: 181–184
Chen G, Huang S, Wei Z, Chen H, Cai J, Qin S, Xie J. 1983. On the tectonic character of Tianshan in Meso-Cenozoic time (in Chinese with English abstract). Geol Rev, 29: 25–30
De Grave J, Glorie S, Buslov M M, Stockli D F, McWilliams M O, Batalev V Y, Van den haute P. 2013. Thermo-tectonic history of the Issyk-Kul basement (Kyrgyz Northern Tien Shan, Central Asia). Gondwana Res, 23: 998–1020
de Jong K, Wang B, Faure M, Shu L, Cluzel D, Charvet J, Ruffet G, Chen Y. 2009. New $^{40}Ar/^{39}Ar$ age constraints on the Late Palaeozoic tectonic evolution of the western Tianshan (Xinjiang, northwestern China), with emphasis on Permian fluid ingress. Int J Earth Sci-Geol Rund, 98: 1239–1258
Dumitru T A, Zhou D, Chang E Z, Graham S A, Hendrix M S, Sobel E R, Carroll A R. 2001. Uplift, exhumation, and deformation in the Chinese Tian Shan. In: Hendrix M S, Davis G A, eds. Paleozoic and Mesozoic Tectonic Evolution of Central Asia: From Continental Assembly to Intracontinental Deformation. Boulder: Geological Society of America Memoir. 71–99
Galbraith R F, Green P F. 1990. Estimating the component ages in a finite mixture. Int J Radiat Appl Instrumentation Part D Nucl Tracks Radiat Measurements, 17: 197–206
Gao J, Qian Q, Long L, Zhang X, Li J, Su W. 2009. Accretionary orogenic process of Western Tianshan, China (in Chinese with English abstract). Geol Bull China, 28: 1804–1816
Garver J I, Brandon M T, Roden-Tice M, Kamp P J J. 1999. Exhumation history of orogenic highlands determined by detrital fission-track thermochronology. Geol Soc Lond Spec Publ, 154: 283–304
Ge R, Zhu W, Wu H, Zheng B, Zhu X, He J. 2012. The Paleozoic northern margin of the Tarim Craton: Passive or active? Lithos, 142-143: 1–15
Glorie S, De Grave J, Buslov M M, Elburg M A, Stockli D F, Gerdes A, Van den haute P. 2010. Multi-method chronometric constraints on the evolution of the Northern Kyrgyz Tien Shan granitoids (Central Asian Orogenic Belt): From emplacement to exhumation. J Asian Earth Sci, 38: 131–146
Glorie S, De Grave J. 2016. Exhuming the Meso-Cenozoic Kyrgyz Tianshan and Siberian Altai-Sayan: A review based on low-temperature thermochronology. Geosci Front, 7: 155–170
Han B F, He G Q, Wang X C, Guo Z J. 2011. Late Carboniferous collision between the Tarim and Kazakhstan-Yili terranes in the western segment of the South Tian Shan Orogen, Central Asia, and implications for the Northern Xinjiang, western China. Earth-Sci Rev, 109: 74–93
Han Y, Zhao G. 2018. Final amalgamation of the Tianshan and Junggar orogenic collage in the southwestern Central Asian Orogenic Belt: Constraints on the closure of the Paleo-Asian Ocean. Earth-Sci Rev, 186: 129–152
He D, Zhou X, Yang H, Lei G, Ma Y. 2009. Geological structure and its controls on giant oil and gas fields in Kuqa Depression, Tarim Basin: A clue from new shot seismic data (in Chinese with English abstract). Geotect Metal, 33: 19–32
He G, Lu H, Yang S, Li S. 2004. Subsiding features of the Mesozoic and Cenozoic Kuqa Basin, Northwestern China (in Chinese with English abstract). J Zhejiang Univ-Sci Ed, 31: 110–113
Huang B, Piper J D A, Peng S, Liu T, Li Z, Wang Q, Zhu R. 2006. Magnetostratigraphic study of the Kuche Depression, Tarim Basin, and Cenozoic uplift of the Tian Shan Range, Western China. Earth Planet Sci Lett, 251: 346–364
Huang H, Wang T, Tong Y, Qin Q, Ma X, Yin J. 2020. Rejuvenation of ancient micro-continents during accretionary orogenesis: Insights from the Yili Block and adjacent regions of the SW Central Asian Orogenic Belt. Earth-Sci Rev, 208: 103255
Jolivet M, Dominguez S, Charreau J, Chen Y, Li Y, Wang Q. 2010. Mesozoic and Cenozoic tectonic history of the central Chinese Tian Shan: Reactivated tectonic structures and active deformation. Tectonics, 29: TC6019
Jolivet M. 2015. Mesozoic tectonic and topographic evolution of Central Asia and Tibet: A preliminary synthesis. Geol Soc Lond Spec Publ, 427: 19–55
Lei J S, Zhao D P. 2007. Teleseismic P-wave tomography and the upper mantle structure of the central Tien Shan orogenic belt. Phys Earth Planet Inter, 162: 165–185
Li S, Wang Q, Li Z, Wang D. 2006. Detrital modes of sandstones and their implications for basin-mountain evolution between the Kuqa Depression and South Tianshan Mountains (in Chinese with English abstract). Chin J Geol, 41: 465–478
Li Z, Guo H, Wang D, Lin W. 2005. Mesozoic-Cenozoic tectonic transition in Kuqa Depression-Tianshan, Northwest China: Evidence from sandstone detrital and geochemical records. Sci China Ser D-Earth Sci, 48: 1387–1402
Li Z, Peng S. 2010. Detrital zircon geochronology and its provenance implications: Responses to Jurassic through Neogene basin-range interactions along northern margin of the Tarim Basin, Northwest China. Basin Res, 22: 126–138
Li Z, Song W, Peng S, Wang D, Zhang Z. 2004a. Mesozoic-Cenozoic tectonic relationships between the Kuqa subbasin and Tian Shan, northwest China: Constraints from depositional records. Sediment Geol, 172: 223–249
Li Z, Wang D, Lin W, Wang Q. 2004b. Mesozoic-Cenozoic clastic composition in Kuqa Depression, northwest China: Implication for provenance types and tectonic attributes (in Chinese with English abstract). Acta Petrol Sin, 20: 655–666
Liu C, Wu C, Gao Y, Lei M, Qin H, Li M. 2014. Zircon LA-ICP-MS U-Pb dating and Lu-Hf isotopic system of A-type granitoids in South Tianshan, Beicheng County, Xinjiang (in Chinese with English abstract). Acta Petrol Sin, 30: 1595–1614
Liu D, Jolivet M, Yang W, Zhang Z, Cheng F, Zhu B, Guo Z. 2013. Latest Paleozoic-Early Mesozoic basin-range interactions in South Tian Shan (northwest China) and their tectonic significance: Constraints from detrital zircon U-Pb ages. Tectonophysics, 599: 197–213
Macaulay E A, Sobel E R, Mikolaichuk A, Kohn B, Stuart F M. 2014. Cenozoic deformation and exhumation history of the Central Kyrgyz Tien Shan. Tectonics, 33: 135–165
Malusà M G, Fitzgerald P G. 2020. The geologic interpretation of the detrital thermochronology record within a stratigraphic framework, with examples from the European Alps, Taiwan and the Himalayas. Earth-Sci Rev, 201: 103074
Morin J, Jolivet M, Barrier L, Laborde A, Li H, Dauteuil O. 2019. Planation surfaces of the Tian Shan Range (Central Asia): Insight on several 100 million years of topographic evolution. J Asian Earth Sci, 177: 52–65
Morin J, Jolivet M, Robin C, Heilbronn G, Barrier L, Bourquin S, Jia Y. 2018. Jurassic paleogeography of the Tian Shan: An evolution driven by far-field tectonics and climate. Earth-Sci Rev, 187: 286–313
Pupin J P. 1980. Zircon and granite petrology. Contrib Mineral Petrol, 73: 207–220
Qin Q. 2017. Geochronology, petrogenesis and tectonic significances of the Paleozoic intrusions in the northern margin of Tarim Craton and the

South Tianshan. Doctoral Dissertation. Beijing: China University of Geosciences-Beijing
Qiu N, Chang J, Li J, Li W, Yun L, Li H. 2012. New evidence on the Neogene uplift of South Tianshan: Constraints from the (U-Th)/He and AFT ages of borehole samples of the Tarim basin and implications for hydrocarbon generation. Int J Earth Sci-Geol Rund, 101: 1625–1643
Tan Z, Agard P, Monié P, Gao J, John T, Bayet L, Jiang T, Wang X S, Hong T, Wan B, Caron B. 2019. Architecture and P-T-deformation-time evolution of the Chinese SW-Tianshan HP/UHP complex: Implications for subduction dynamics. Earth-Sci Rev, 197: 102894
Tang L, Jin Z, Jia C, Pi X, Chen S, Xie H, Wang Z. 2004. A large-scale salt nappe complex in the leading edge of the Kuqa foreland fold-thrust belt, Tarim Basin, Northwest China (in Chinese with English abstract). Acta Geol Sin, 78: 17–25
Vermeesch P. 2018. IsoplotR: A free and open toolbox for geochronology. Geosci Front, 9: 1479–1493
Wang B, Shu L, Faure M, Jahn B, Cluzel D, Charvet J, Chung S, Meffre S. 2011. Paleozoic tectonics of the southern Chinese Tianshan: Insights from structural, chronological and geochemical studies of the Heiyingshan ophiolitic mélange (NW China). Tectonophysics, 497: 85–104
Wang Q, Li S, Du Z. 2009. Differential uplift of the Chinese Tianshan since the Cretaceous: Constraints from sedimentary petrography and apatite fission-track dating. Int J Earth Sci-Geol Rund, 98: 1341–1363
Wang Q, Zhang P Z, Freymueller J T, Bilham R, Larson K M, Lai X, You X, Niu Z, Wu J, Li Y, Liu J, Yang Z, Chen Q. 2001. Present-day crustal deformation in China constrained by global positioning system measurements. Science, 294: 574–577
Wang X S, Klemd R, Gao J, Jiang T, Zhang X. 2020. Early Devonian tectonic conversion from contraction to extension in the Chinese Western Tianshan: A response to slab rollback. Geol Soc Am Bull, 133: 1613–1633
Xiao W J, Zhang L, Qin K, Sun S, Li J. 2004. Paleozoic accretionary and collisional tectonics of the eastern Tianshan (China): Implications for the continental growth of Central Asia. Am J Sci, 304: 370–395
Yang G, Qian X. 1995. Subsidence of the Kuqa Depression and Mesozoic-Cenozoic structural reactivations in Tianshan (in Chinese with English abstract). Xinjiang Geol, 13: 264–273
Yang S, Chen H, Cheng X, Xiao A, Zhou Y, Lu H, Jia C, Wei G. 2003. Cenozoic uplifting and unroofing of Southern Tianshan, China (in Chinese with English abstract). J Nanjing Univ, 39: 1–8
Yin A, Nie S, Craig P, Harrison T M, Ryerson F J, Xianglin Q, Geng Y. 1998. Late Cenozoic tectonic evolution of the southern Chinese Tian Shan. Tectonics, 17: 1–27
Yin J, Chen W, Hodges K V, Xiao W, Cai K, Yuan C, Sun M, Liu L P, van Soest M C. 2018. The thermal evolution of Chinese central Tianshan and its implications: Insights from multi-method chronometry. Tectonophysics, 722: 536–548
Zhu Z. 2007. Geological composition and tectonic evolution of the South Tianshan, Xinjiang (in Chinese with English abstract). Doctoral Dissertation. Beijing: Chinese Academy of Geological Sciences

(Responsible editor: Yuanbao WU)